られ、進行性病変と分類した。

Sacrifice weeks	発症率　　(%)	大動脈硬化病変所見
負荷前	1 / 7　例中　(14%)	初期病変
負荷8週	7 / 7　例中　(100%)	進行性病変
負荷16週	4 / 4　例中　(100%)	複合性病変

表 1. 動脈硬化病変の進行度に基づいた分類。

高コレステロール食餌を与えた AN-KO マウスの大動脈では、負荷前の 1 例に初期病変が認められたが、残りの 6 例は正常所見であった。負荷 8 週では進行性病変を、負荷 16 週では複合病変を全例に認めた。負荷 16 週における複合病変は石灰化や血管内腔を狭窄するものが主体であった。

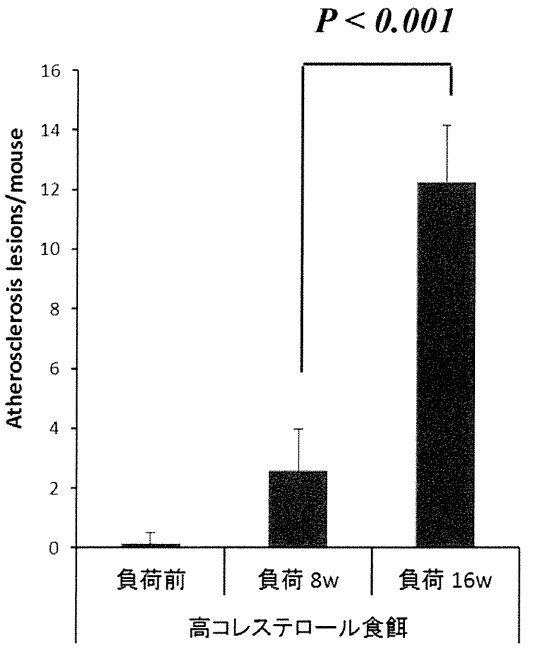

図 5. 動脈硬化病変数の解析。

高コレステロール食餌を与えた AN-KO マウス大動脈の HE および EVC 染色標本を病理組織学的に観察し、マウス 1 匹当たりの動脈硬化病変の発生個数を算出した。その結果、負荷週数の増加と共に、病変数も増加し、16 週では 8 週に比し、有意に増加した。

A　Wild type マウス　　B　ApoE-KO マウス

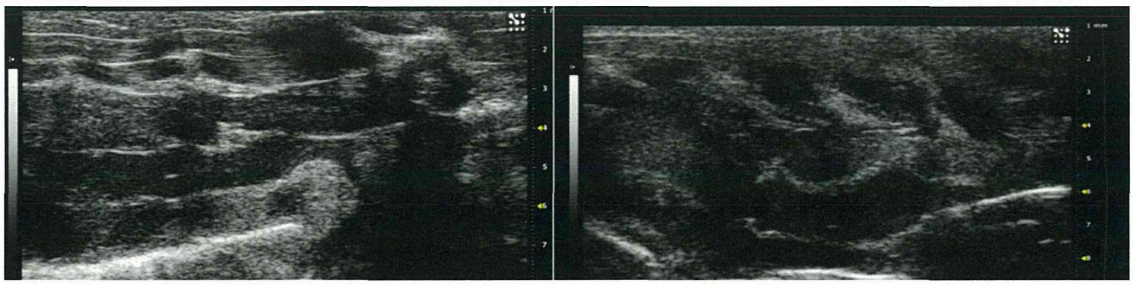

C

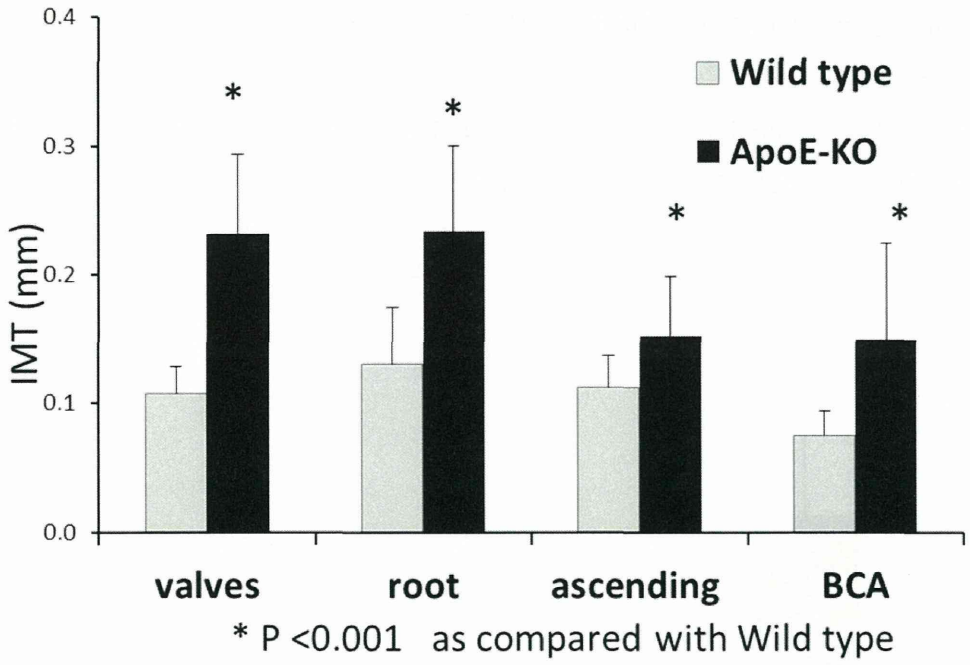

図 6. A, B: 超音波断層における上行大動脈の長軸断層像。

ApoE-KO マウスの上行大動脈血管壁の肥厚を認めた（B)。Wild type の大動脈は正常所見であった（A)。C: 上行大動脈の超音波長軸断層像における血管壁の IMT 値。ApoE-KO マウスの valves（大動脈弁), root（大動脈起始部), ascending（上行大動脈）および BCA（腕頭動脈）の位置での IMT 値は、Wild type より有意に高値であった。

A　　B

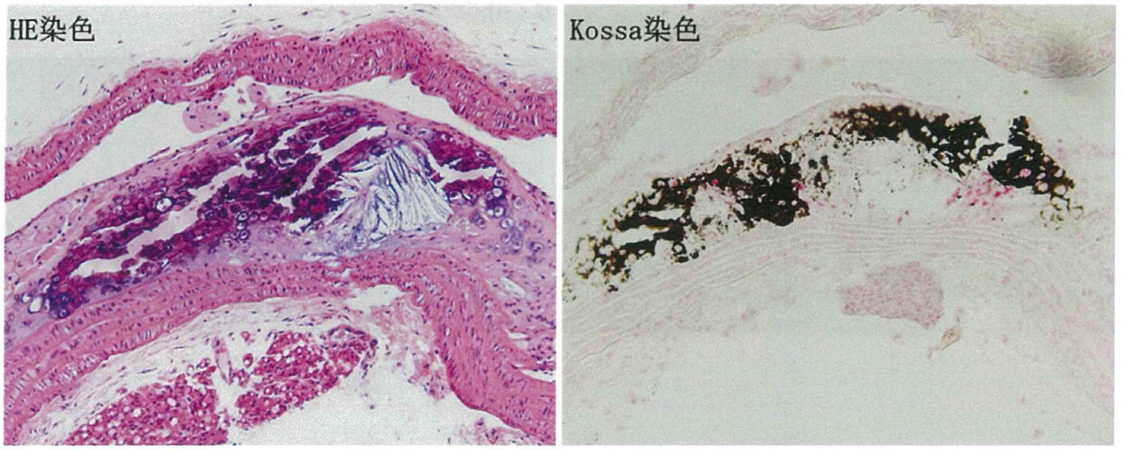

図 7. 動脈硬化の複合病変における石灰化の証明（Kossa 染色）。

A: HE 染色,　B: Kossa 染色

ApoE-KO マウスの動脈硬化病変部内に、Kossa 反応陽性部位が観察され、カルシウム沈着であることを確認し、石灰化を伴う複合病変と分類した。

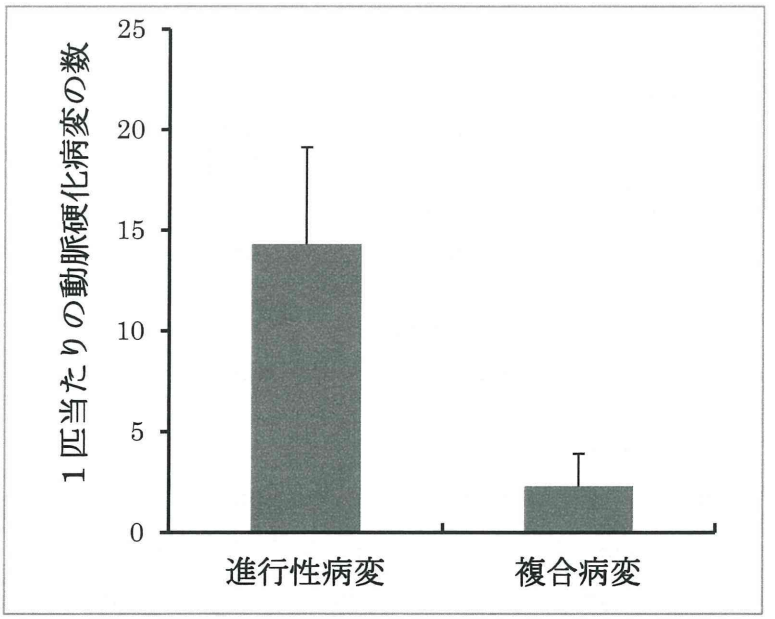

図 8. 動脈硬化病変の発生個数。

高コレステロール食を 16 週間摂取させた ApoE-KO マウスの動脈硬化病変を進行度に基づいて分類し、マウス 1 匹当たりの病変の発生個数で表した。

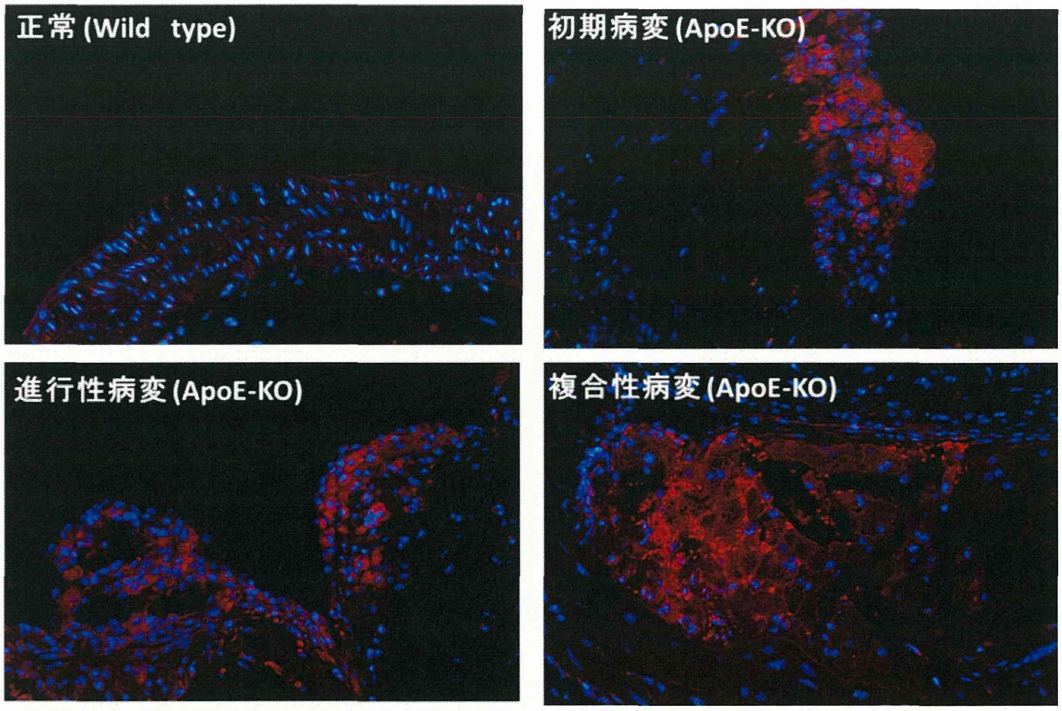

図 9. 動脈硬化病変のマクロファージ集簇（抗 F4/80 抗体の免疫蛍光染色）。
動脈硬化病変の初期病変から複合病変に至るまでマクロファージの集簇がみられた。

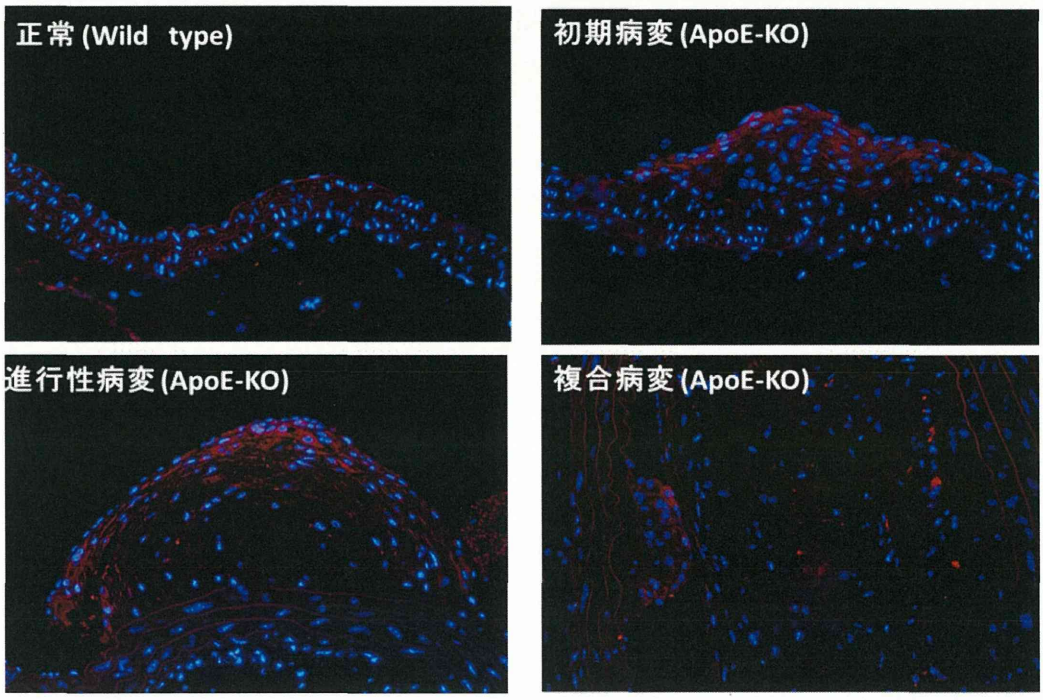

図 10. 動脈硬化病変のテネイシン C の発現（抗テネイシン C 抗体の免疫蛍光染色）。
動脈硬化病変の初期病変から複合病変に至るまでテネイシン C の発現が観察された。

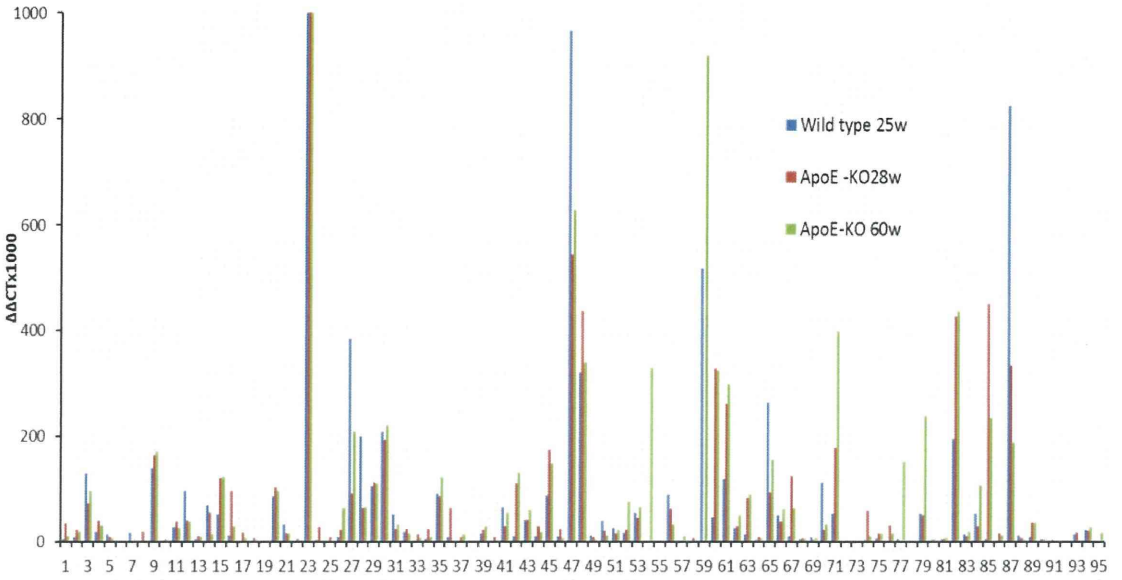

図 11. プライマーアレイを用いた Real time PCR による動脈硬化病変の網羅的解析。
ホルマリン固定のパラフィン包埋されたマウスの大動脈組織から mRNA を抽出し、96 種類のサイトカインに対するプライマーアレイを用いて、Real time PCR による動脈硬化病変の網羅的な解析を行った。ApoE-KO マウスの動脈硬化病変では、Wild type マウスの正常大動脈に比較して、幾つかのサイトカインで mRNA の発現が著しく上昇していた。

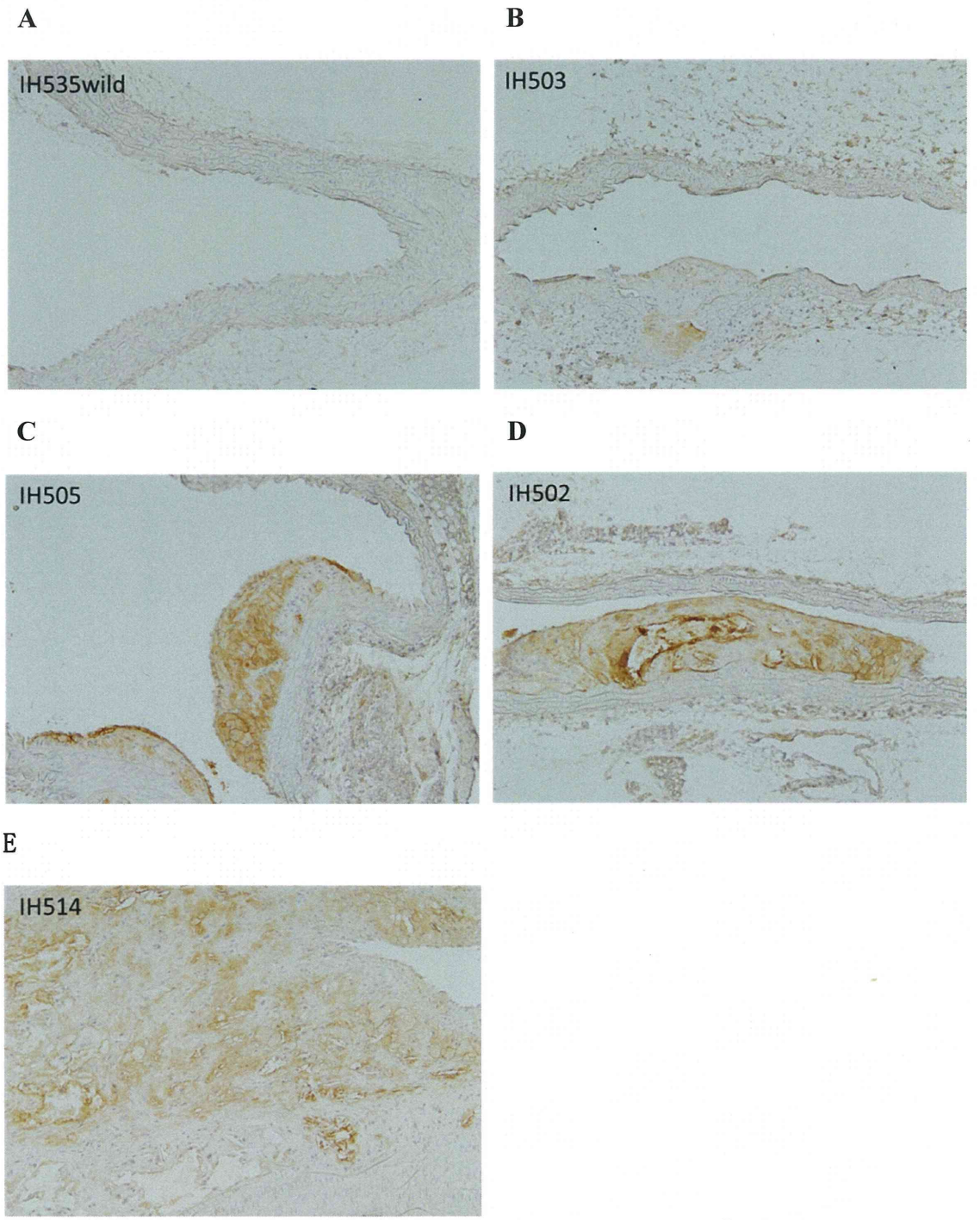

図 12. 動脈硬化病変の Cxcl16 発現（抗 Cxcl16 抗体を用いた免疫組織学的染色)。
A: Wild type, B～E: ApoE-KO マウス。Wild type のマウスでは全く Cxcl16 の発現は認められなかった(A)。 ApoE-KO マウスの動脈でも正常部位では Cxcl16 の発現は観察されなかったが（B)、動脈硬化病変では進行性病変や複合病変でその発現が観察された（C-E)。

A

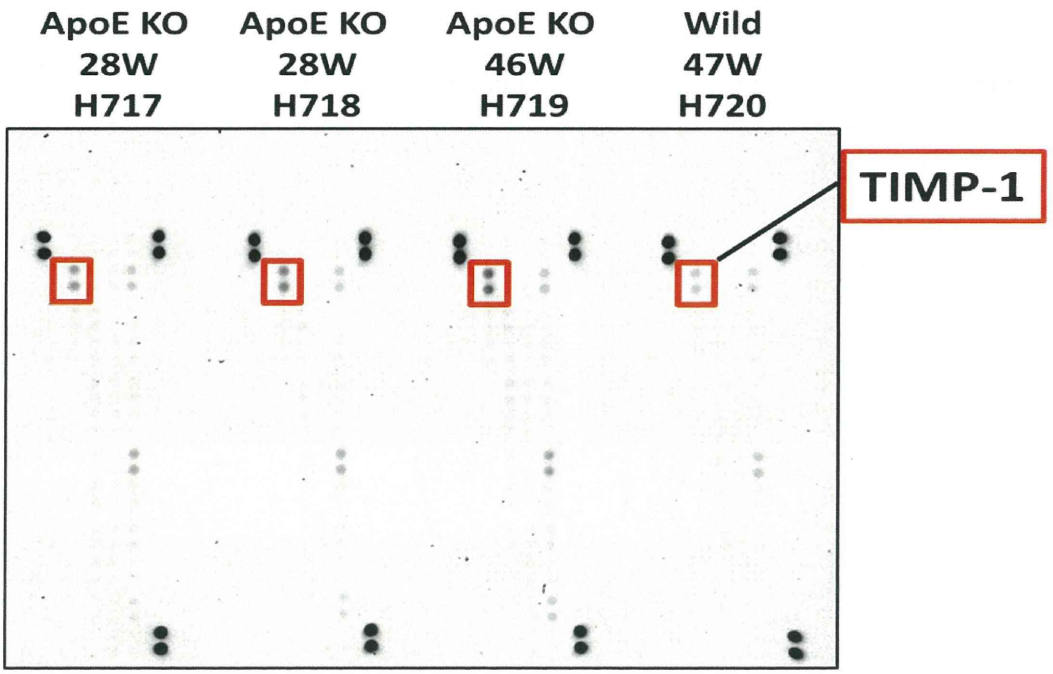

B

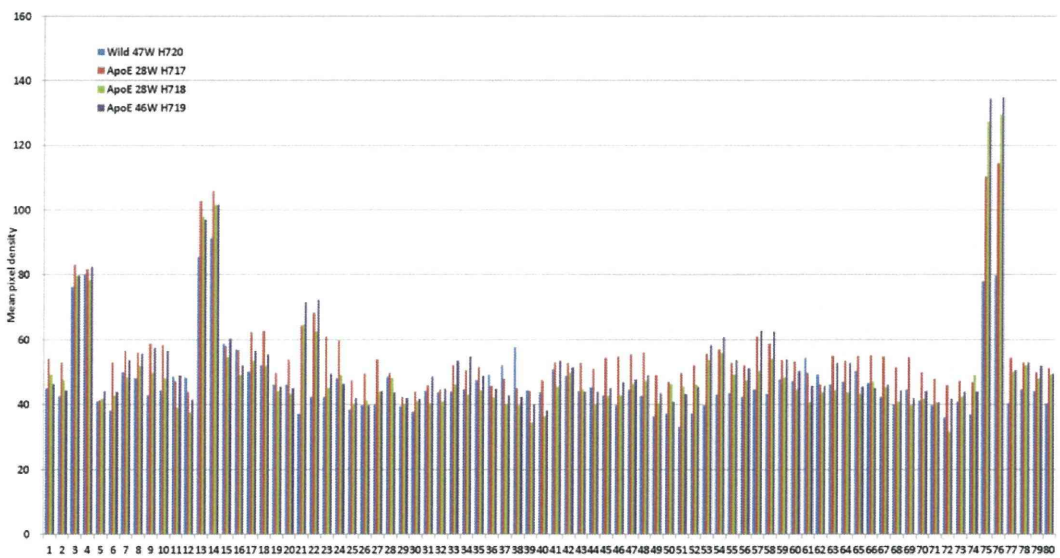

図 13 動脈組織 からの抽出タンパクを用いた抗体アレイ解析。

A: ニトロセルロース膜上に 40 種類のサイトカイン関連の抗体が固相化してあり、TIMP-1 では、Wild type に比較して、ApoE-KO マウスにおいて発現が上昇していた。B: 抗体アレイの解析結果。発現スポットの density をデジタル画像解析ソフト Image J で測定した。

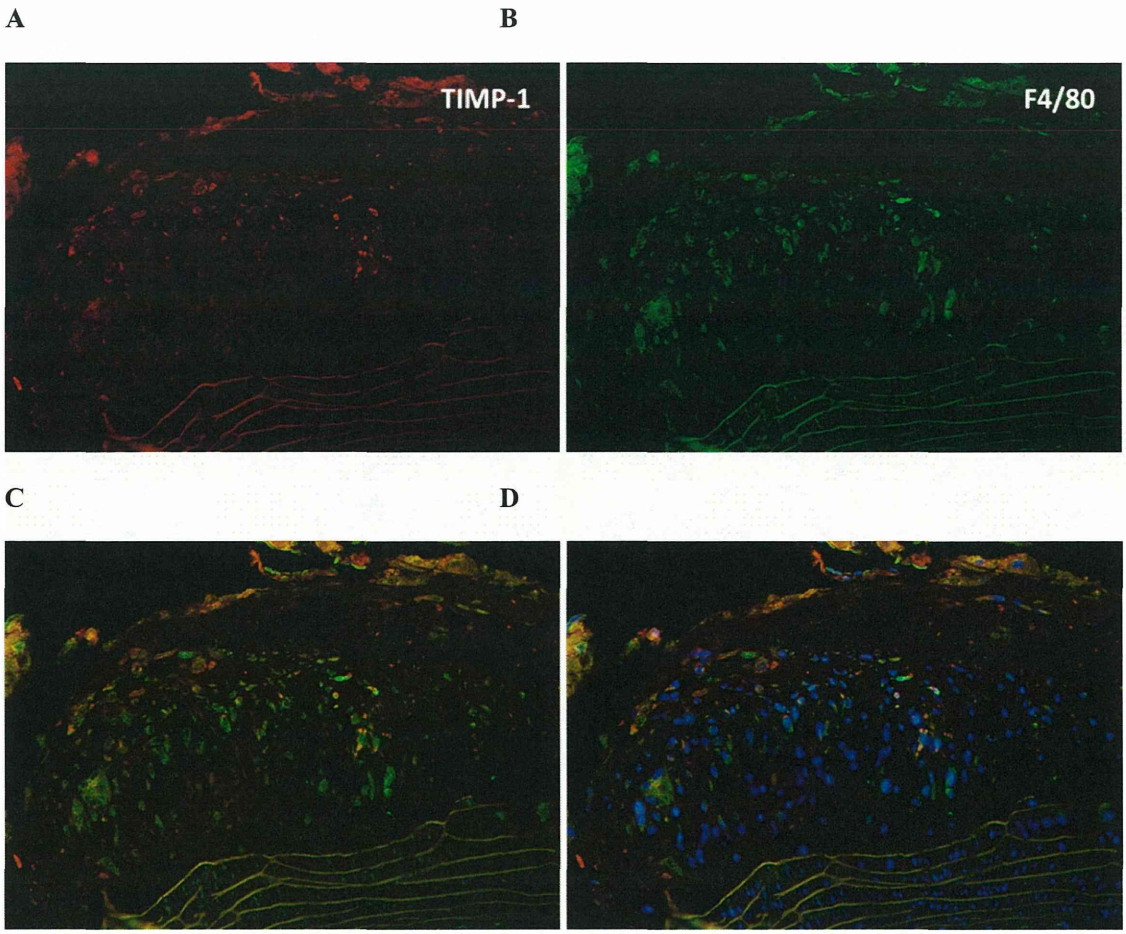

図 14. ApoE-KO マウスの動脈硬化病変に対する TIMP-1 抗体と F4/80 抗体の二重免疫蛍光染色。

A：TIMP-１発現が脂質コアの部位に観察された（抗 TIMP-１抗体免疫蛍光染色)。B：マクロファージの集簇が脂質コアの部位に認められた（抗 F4/80 抗体免疫蛍光染色)。C: TIMP-1 発現とマクロファージ集簇と重ね合わせ、オレンジ色を呈している箇所が TIMP-1 を有しているマクロファージであり、殆どの TIMP-1 はマクロファージ内に局在していることが分かる（抗 TIMP-1 抗体 と抗 F4/80 抗体の二重免疫蛍光染色)。 D: C の画像にさらに DAPI 核染色像を merge した（DAPI)。

A　　B

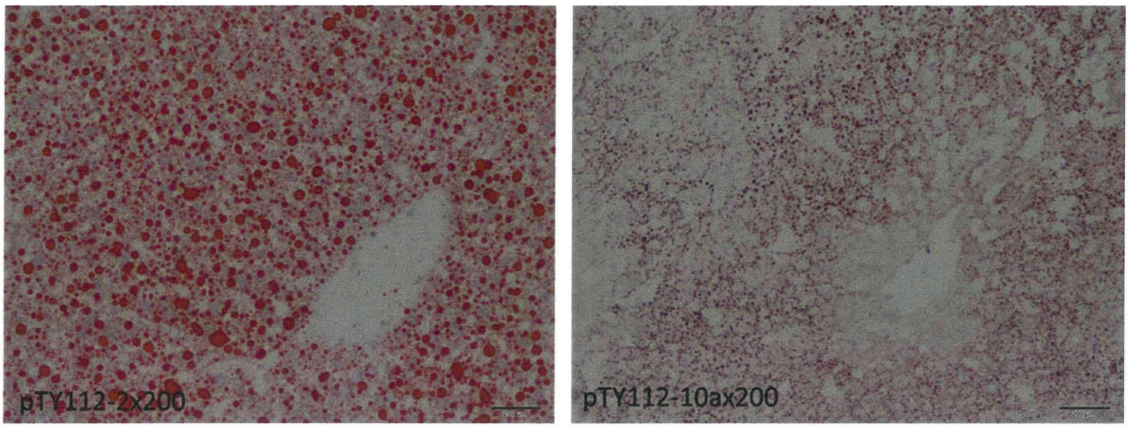

図 15.　脂肪肝に対する Oil Red 染色（C57BL/6J マウス, Oil red O 脂肪染色)。

A: Saline、B: ApoC3-01S 20 mg/kg。

アンチセンス ApoC3-01S 20 mg/kg 投与群で、病理組織学的に脂肪肝の減少が観察され、Oil Red 染色により、対照群に比較して(A)、肝細胞での脂肪の蓄積が著しく減少(B)していることを示した（Yamamoto T, et al　European Journal of Pharmacology, 723, 353-359, 2014)。

別紙４

研究成果の刊行に関する一覧表レイアウト

雑誌

発表者氏名	論文タイトル名	発表誌名	巻号	ページ	出版年
Morihiro K, Kodama T, Mori S, Obika S	Photoinduced Changes in Hydrogen Bonding Patterns of 8-Thiopurine Nucleobase Analogues in a DNA Strand	Orgamic & Biomolecular Chemistry	12	2468-2473	2014年
Shrestha A. R, Kotobuki Y, Hari Y, Obika S	Guanidine Bridged Nucleic Acid (GuNA): An Effect of Cationic Bridged Nucleic Acid on DNA Binding Affinity	Chem Commun	50	575-577	2014年
Morihiro K, Kodama T, Waki R, Obika S	Light-triggered Strand Exchange Reaction Using the Change in the Hydrogen Bonding Pattern of the Nucleobase Analog	Chemical Science	5	744-750	2014年
Yamamoto T, Obika S, Nakatani M, Yasuhara H, Wada F, Shibata E, Shibata MA, Harada-Shiba M	Locked Nucleic Acid Antisense Inhibitor Trageing Apolipoprotein C-III Efficiently and Preferentially Removes Tryglyceride from Large Very Low-density Lipoprotein Particles in Murine Plasma	European Journal of Pharmacology	723	353-359	2014年
Hari Y, Nakahara M, Ijitsu S, Obika S	The Ability of 1-Aryltriazole-containing Nucleobases to Recognize a TA Base Pair in Triplex DNA	Heterocycles	88	377-386	2014年
Hari Y, Morikawa T, Osawa T, Obika S	Synthesis and Properties of 2'-*O*,4'-*C*-Ethyleneoxy Bridged 5-Methyluridine	Organic Letters	15	3702-3705	2013年
Hari Y, Akabane M, Obika S	2',4'-BNA Bearing a Chiral Guanidinopyrrolidine-containing Nucleobase with Potent Ability to Recognize the CG Base Pair in Parallel-motif DNA Triplex	Chem Comm	49	7421-7423	2013年
Akiyama H, Miyashita K, Hari Y, Obika S, Imanishi T	Synthesis of Novel Polyesteramine Dendrimers by Divergent and Convergent Methods	Tetrahedron	33	6810-6820	2013年

Hari Y, Nakahara M, Obika S	Triplex-forming Ability of Oligonucleotides Containing 1-Aryl-1,2,3-Triazole Nucleobases Linked via a Two Atom-length Spacer	Bioorganic & Medicainal Chemistry	21	5583-5588	2013年
Hari Y, Kashima S, Inohara H, Ijitsu S, Imanishi T, Obika S	Base-pair Recognition Ability of Hydroxyphenyl Nucleobases in Parallel Triplex DNA	Tetrahedron	69	6381-6391	2013年
Hari Y, Osawa T, Kotobuki Y, Yahara, A Shrestha A. R, Obika S	Synthesis and Properties of Thymidines with Six-membered Amide Bridge	Bioorganic & Medicainal Chemistry	21	4405-4412	2013年
Morihiro K, Kodama T, Kentefu, Moai Y, Veedu R. N, Obika S	Selenomethylene-Locked Nucleic Acid Enables Reversible Hybridization in Response to Redox Changes	Angewandte Communications	52	5074-5078	2013年
Tsuji M, Taguchi A, Ohshima M, Kasahara Y, Sato Y, Tsuda H, Otani K, Yamahara K, Ihara M, Harada-Shiba M, Ikeda T, Matsuyama T	Effects of intravenous administration of umbilical cord blood $CD34^+$ cells in a mouse model of neonatal stroke	Neuroscience	263C	14-158	2014年
Yuasa Y, Osaki T, Makino H, Iwamoto N, Kishimoto I, Usami M, Harada-Shiba M	Proeomic analysis of proteins eliminated by LDL-apheresis	Therapeutic Apheresis and Dialysis	18(1)	93-102	2014年
Yokoyama S, Ueshima H, Miida T, Nakamura M, Takata K, Fukukawa T, Goto T, Harada-Shiba M, Sano M, Kato K, Matsuda K	High-density lipoprotein levels have markedly increased over the past twenty years in japan	Journal of Atherosclerosis and Thrombosis	21(2)	151-160	2014年
Shibata MA, Shibata E, Morimoto J, Harada-Shiba M	Therapy with siRNA for Vegf-c but Not for Vegf-d Suppresses Wide-spectrum Organ Metastasis in an Immunocompetent Xenograft Model of Metastatic Mammary Cancer	Anticancer Research	33	4237-4248	2013年

Kobayashi K, Nagata E, Sasaki K, Harada-Shiba M, Kojo S, Kikuzaki H	Increase in Secretory Sphingomyelinase Activity and Specific Ceramides in the Aorta of Apolipoprotein E Knockout Mice during Aging, Biol	Biol. Pharm. Bull	36(7)	1192-1196	2013年
Makino H, Harada-Shiba M	New aspects of statin therapy	IEMAMC	13	97-106	2013年
Terasaki F, Morita H, Harada-Shiba M, Ohta N, Otsuka K, Nogi S, Miyamura M, Suzuki S, Ito T, Shimomura H, Katsumata T, Miyamoto Y, Ishizaka N	Familial Hypercholesterolemia with Multiple Large Tendinous Xanthomas and Advanced coronary Artery Atherosclerosis	Internal Medicine	52	577-581	2013年

Organic & Biomolecular Chemistry

PAPER

View Article Online
View Journal | View Issue

Photoinduced changes in hydrogen bonding patterns of 8-thiopurine nucleobase analogues in a DNA strand†

Cite this: Org. Biomol. Chem., 2014, 12, 2468

Kunihiko Morihiro,[a,b] Tetsuya Kodama,[c] Shohei Mori[a] and Satoshi Obika*[a,b]

Received 5th December 2013,
Accepted 13th February 2014

DOI: 10.1039/c3ob42427h

www.rsc.org/obc

Hydrogen bonds (H-bonds) formed between nucleobases play an important role in the construction of various nucleic acid structures. The H-donor and H-acceptor pattern of a nucleobase is responsible for selective and correct base pair formation. Herein, we describe an 8-thioadenine nucleobase analogue and an 8-thiohypoxanthine nucleobase analogue with a photolabile 6-nitroveratryl (NV) group on the sulfur atom (**SA**^{NV} and **SH**^{NV}, respectively). Light-triggered removal of the NV group causes tautomerization and a change in the H-bonding pattern of **SA**^{NV} and **SH**^{NV}. This change in the H-bonding pattern has a strong effect on base recognition by 8-thiopurine nucleobase analogues. In particular, base recognition by **SH**^{NV} is clearly shifted from guanine to adenine upon photoirradiation. These results show that a photoinduced change in the H-bonding pattern is a unique strategy for manipulating nucleic acid assembly with spatiotemporal control.

Introduction

The complementarity of natural A–T and G–C base pairs in DNA is the principal mechanism for the preservation and flow of genetic information. The hydrogen-bonding (H-bonding) patterns of the four natural nucleobases play an important role in the selective and correct formation of base pairs. These H-bonding interactions can result in the formation of higher order complexes of nucleic acids, depending on the sequence. Therefore, the control of H-bonding interactions using external stimuli is important for regulating biological processes and for the possibility of developing unique DNA-based molecular machines. Various external stimuli have been used to this end; light is an ideal trigger because the timing, location, and intensity of the irradiation can be easily controlled. Among such strategies, nucleobase caging strategies involving the installation of a photolabile group are very important. Photolabile caging groups perturb the H-bonding capabilities of the nucleobases. Photoirradiation reinstates the H-bonding capabilities and allows nucleobase interaction in the "OFF to ON" direction. Nucleobase-caged nucleosides can be widely used for the photoregulation of antisense oligodeoxynucleotides (ODNs),[1,2] siRNAs,[3,4] aptamers,[5] ribozymes[6,7] and deoxyribozymes,[8,9] diagnostic ODNs,[10] DNA architectures,[11] and DNA logic gates.[12,13]

Recently, we reported the synthesis and properties of a unique light-responsive nucleobase analogue derived from 2-mercaptobenzimidazole (**SB**^{NV}) (Fig. 1a).[14] **SB**^{NV} is modified with a photolabile 6-nitroveratryl (NV) group,[15] and the nitrogen at the 3-position serves as an H-acceptor (A). **SB**^{NV} can selectively form a base pair with guanine even before photoirradiation, unlike conventional caged nucleobases. Light-triggered removal of the NV group causes tautomerization of the nucleobase, and changes the role of the 3-nitrogen atom from H-A to H-donor (D). Following this change in the H-bonding pattern, base recognition by **SB**^{NV} can be shifted from guanine to adenine. We also demonstrated that a light-triggered strand exchange reaction targeting different mRNA fragment sequences could be achieved using ODNs containing **SB**^{NV}. These results indicate that a photoinduced change in the H-bonding pattern of a nucleobase is a good strategy for manipulating nucleic acid assemblies in a spatially and temporally controlled manner. In this paper, to further investigate the effect of this change in H-bonding pattern of nucleobases on the base recognition ability, we designed new light-responsive nucleoside analogues bearing the NV group: 8-thioadenine and 8-thiohypoxanthine (**SA**^{NV} and **SH**^{NV}, respectively;

[a]Graduate School of Pharmaceutical Sciences, Osaka University, 1-6 Yamadaoka, Suita, Osaka 565-0871, Japan. E-mail: obika@phs.osaka-u.ac.jp; Fax: +81 6-6879-8204; Tel: +81 6-6879-8200
[b]National Institute of Biomedical Innovation (NIBIO), 7-6-8 Saito-Asagi, Ibaraki, Osaka 567-0085, Japan
[c]Graduate School of Pharmaceutical Sciences, Nagoya University, Furo-cho, Chikusa-ku, Nagoya, Aichi 464-8601, Japan

†Electronic supplementary information (ESI) available: NMR spectra of new compounds, HPLC and MALDI-TOF MS analysis of modified ODNs, photoreaction of modified ODNs and UV melting curves for modified duplexes. See DOI: 10.1039/c3ob42427h

This journal is © The Royal Society of Chemistry 2014

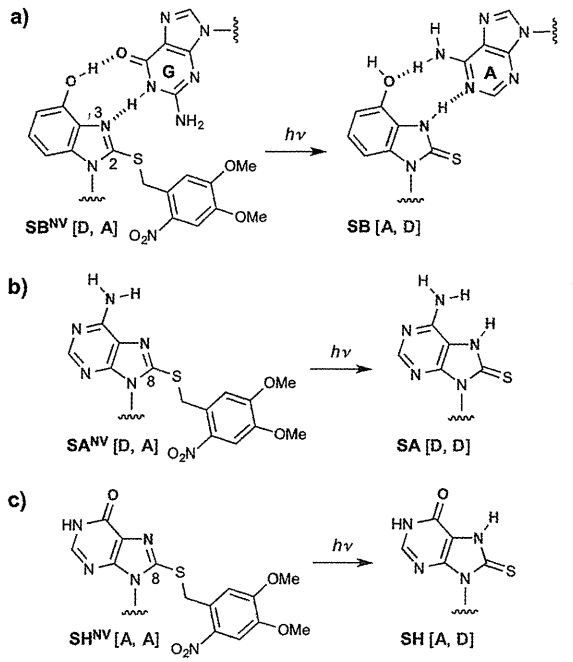

Fig. 1 (a) Change in base recognition by SB^{NV} upon photoirradiation. (b) Photoinduced changes in hydrogen bonding patterns of SA^{NV} and (c) SH^{NV}.

Fig. 1b and c). 8-Thiopurine analogues should preferentially adopt the *syn* conformation about the glycosidic bond due to steric repulsion between the C8-sulfur atom and the 4′-oxygen atom in the *anti* conformer.[16,17] SA^{NV} and SH^{NV} should also adopt the *syn* conformation and use the H-A and H-D Hoogsteen face to contact the target base. The H-bonding pattern of SA^{NV} and SH^{NV} at the Hoogsteen face would thus be changed from [D, A] to [D, D] and [A, A] to [A, D], respectively (Fig. 1). T_m evaluation of modified ODNs revealed that photoinduced changes in H-bonding patterns of 8-thiopurine nucleobase analogues have a pronounced effect on base recognition abilities.

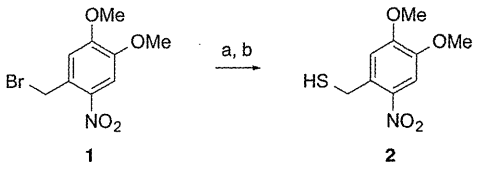

Scheme 1 Preparation of 6-nitroveratrylthiol **2**. *Reagents and conditions*: (a) KSAc, THF, rt; (b) conc. HCl aq., MeOH, 60 °C, 94% over two steps.

Results and discussion

The syntheses of the phosphoramidites bearing SA^{NV} and SH^{NV} as a nucleobase are summarized in Scheme 1. 6-Nitroveratrylthiol (**2**) was prepared from 6-nitroveratrylbromide (**1**) (Scheme 1) and subjected to reaction with 8-bromo-2′-deoxyadenosine derivative (**3**)[18] to afford **4** (Scheme 2). Phosphitylation at the 3′-hydroxyl group provided SA^{NV}-phosphoramidite **5**. For the preparation of SH^{NV}-phosphoramidite **9**, 8-bromoinosine (**6**)[19] was treated with **2** to give **7** (Scheme 3). Tritylation of the primary hydroxyl group in **7** and phosphitylation of the secondary hydroxyl group provided phosphoramidite **9**. Amidite blocks **5** and **9** were applied to an automated DNA synthesizer to incorporate SA^{NV} and SH^{NV} into ODNs. SA^{NV} and SH^{NV} were incorporated into the middle of the pyrimidine

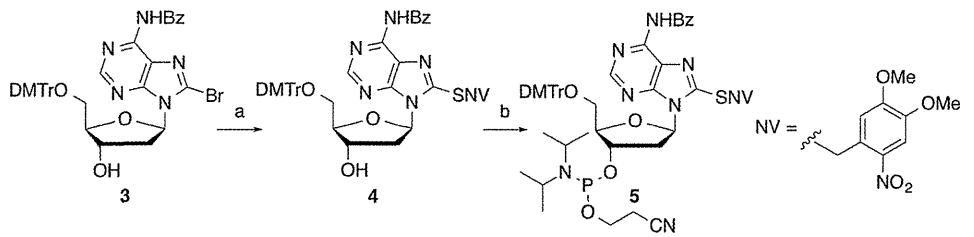

Scheme 2 Preparation of the phosphoramidites bearing SA^{NV}. *Reagents and conditions*: (a) **2**, K_2CO_3, DMF, rt, 52%; (b) $(iPr_2N)P(Cl)O(CH_2)_2CN$, iPr_2NEt, MeCN, rt, 77%.

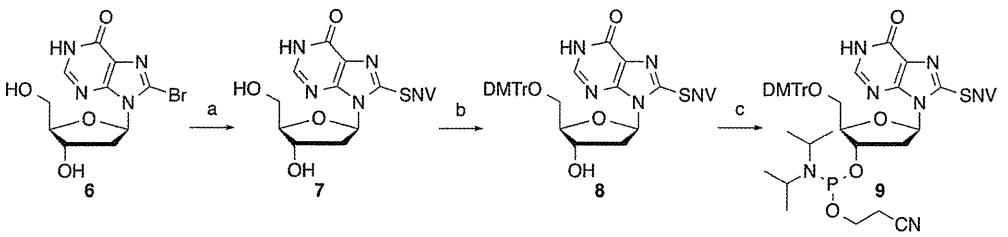

Scheme 3 Preparation of the phosphoramidites bearing SH^{NV}. *Reagents and conditions*: (a) **2**, K_2CO_3, DMF, rt, 25%; (b) DMTrCl, pyridine, rt, 85%; (c) $(iPr_2N)P(Cl)O(CH_2)_2CN$, iPr_2NEt, MeCN, rt, 74%.

10 5'-d(TCGTTT**SA^{NV}**TTGCG)-3'
11 5'-d(TCGTTT**SH^{NV}**TTGCG)-3'
12 5'-d(TCGTTTA TTGCG)-3'
13 5'-d(TCGTTTG TTGCG)-3'
14 3'-d(AGCAAAA AACGC)-5'
15 3'-d(AGCAAAG AACGC)-5'
16 3'-d(AGCAAAC AACGC)-5'
17 3'-d(AGCAAAT AACGC)-5'

Fig. 2 ODN sequences used in this study.

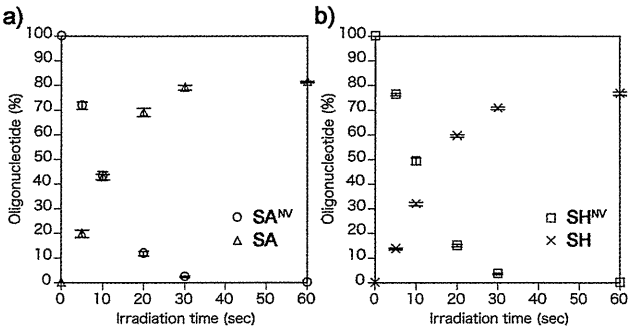

Fig. 3 Time course conversion of (a) **SA^{NV}** to **SA** in ODN **10** and (b) **SH^{NV}** to **SH** in ODN **11** by photoirradiation. Conditions: each ODN (0.1 nmol, 10 μM), sodium phosphate buffer (pH 7.2, 25 mM). Irradiation (365 nm) was performed at rt. Error bars indicate standard deviation (n = 3).

(T) strand of ODN **10** and ODN **11**. After cleavage from the resin and purification by reversed-phase (RP) HPLC, the structure of each ODN was confirmed by MALDI-TOF MS analysis. The sequence of each ODN used in this study is shown in Fig. 2.

The photoreactivity of **SA^{NV}** and **SH^{NV}** in a DNA strand was investigated by RP-HPLC analysis using ODN **10** and ODN **11**. When irradiated at 365 nm at 37 °C, ODN **10** and ODN **11** gradually disappeared. MALDI-TOF MS showed that the resulting ODNs were **SA**-/**SH**-ODNs and confirmed that the NV group of **SA^{NV}** and **SH^{NV}** was efficiently removed. Fig. 3 shows the percentage of the remaining **SA^{NV}**-/**SH^{NV}**- and resulting **SA**-/**SH**-ODNs at several irradiation time points. The photoreaction was complete within 60 s for both ODNs, and the yield of NV-removed ODNs was estimated from the HPLC peak area to be about 80%.

The effects of photoinduced changes in H-bonding patterns of **SA^{NV}** and **SH^{NV}** on their base recognition ability were examined by measuring the T_m values of DNA duplexes containing ODN **10** and ODN **11** (Table 1). ODN **10** and ODN **11** were individually hybridized to four ODNs, generating eight distinct duplexes in which each nucleobase analogue was paired with all possible natural nucleobases. For comparison, naturally matched duplexes containing the A:T and G:C base pairs in the same position were also examined. The duplex containing the **SA^{NV}**:G pair showed the highest T_m value of all the combinations of **SA^{NV}** with other nucleobases ($\Delta T_m \geqq 3$ °C). The

Table 1 T_m values of DNA duplexes[a]

5'-d(GCGTT**X**TTTGCT)-3'
3'-d(CGCAA**Y**AAACGA)-5'

Duplex	X:Y	T_m (°C) UV (−)	T_m [b] (°C) UV (+)
10:14	**SA^{NV}**:A	26	24
10:15	**SA^{NV}**:G	35	28
10:16	**SA^{NV}**:C	24	26
10:17	**SA^{NV}**:T	32	32
11:14	**SH^{NV}**:A	31	39
11:15	**SH^{NV}**:G	35	26
11:16	**SH^{NV}**:C	30	31
11:17	**SH^{NV}**:T	26	28
12:17	A:T	41	41
13:16	G:C	43	43
12:15	A:G (mismatch)	33	33
12:16	A:C (mismatch)	29	29
13:14	G:A (mismatch)	32	32
13:17	G:T (wobble)	35	35

[a] Conditions: each ODN (4.0 μM), NaCl (20 mM), sodium phosphate buffer (10 mM, pH 7.2). [b] T_m values of DNA duplexes after irradiation (365 nm) at 37 °C for 5 min.

SA^{NV}:G pair was slightly less stable than natural base pairs, and its stability was similar to the stability of the G:T wobble base pair. After photoirradiation at 365 nm for 5 min, **SA** showed the highest affinity towards thymine ($\Delta T_m \geqq 4$ °C); however, the T_m values of duplexes containing **SA** are, on the whole, low ($T_m \leqq 32$ °C). **SH^{NV}** in ODN **11** showed the highest affinity towards guanine, similar to **SA^{NV}** ($\Delta T_m \geqq 4$ °C). The T_m value of the duplex containing the **SH^{NV}**:G base pair was also slightly lower than that of natural duplexes. In contrast, after irradiation, the preferred base-pairing partner for **SH^{NV}** clearly changed to adenine ($\Delta T_m \geqq 8$ °C). Notably, the stability of **SH**:A was comparable to that of the natural A:T base pair. These results suggest that photoirradiation induces a change in base recognition by **SH^{NV}** from guanine to adenine. Fig. 4 illustrates the changes in the UV melting profiles of ODN-**11**-formed DNA duplexes and clearly indicates that the change in base recognition by **SH^{NV}** is triggered by photoirradiation.

Although further conclusive experiments such as NMR or X-ray structural analysis are needed to elucidate the precise base pair structures, the results of the T_m measurements suggest that **SA^{NV}** and **SH^{NV}** recognize guanine *via* two H bonds on the Hoogsteen face, as shown in Fig. 5. The stabilities of the **SA^{NV}** and **SH^{NV}**:G base pairs were slightly lower than that of the natural base pairs. It would appear that steric repulsion between the 8-sulfur atom in **SA^{NV}** and the 2-amino group in guanine decreases the stability of the **SA^{NV}**:G pair (Fig. 5a). This observation is consistent with previous reports showing that the base pair between 2-thiouracil and 2,6-diaminopurine is significantly destabilized because of steric hindrance.[20,21] Also, **SH^{NV}** may form a wobble pair with guanine similar to the U:G mismatch pair commonly found in RNA[22] (Fig. 5b); therefore, the **SH^{NV}**:G pair is less stable than natural base pairs. Light-induced changes in H-bonding patterns have profound effects on the base recognition abilities of 8-

This journal is © The Royal Society of Chemistry 2014

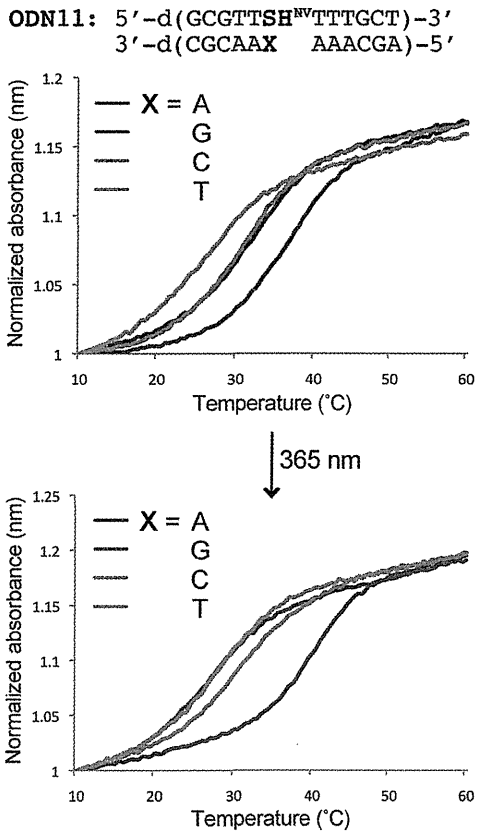

Fig. 4 Light-triggered changes in the denaturation profiles of duplexes containing ODN **11** determined by correlating the absorbance at 260 nm *vs.* temperature. Conditions as given in Table 1.

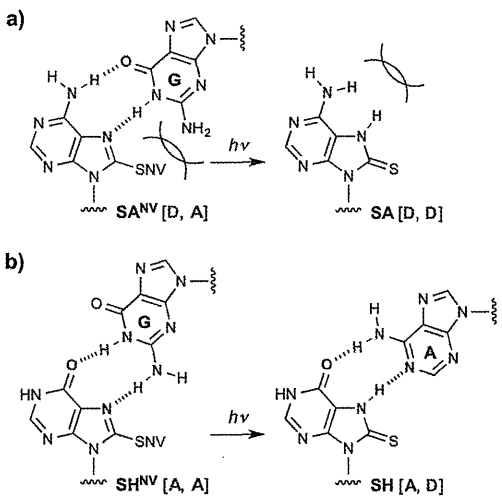

Fig. 5 Plausible change in base recognition by SA^{NV} and SH^{NV} upon photoirradiation.

thiopurine nucleobase analogues. ODN containing **SA** showed low recognition ability toward any nucleobase; this can be explained by the fact that **SA** has an H-bonding [D, D] pattern on the Hoogsteen face, but no natural nucleobase has an [A, A] pattern for base pair formation with **SA** (Fig. 5a). **SA** can interact with thymine using its Watson–Crick face in the *anti*-conformation; however, the resulting poor base-recognition-ability indicated that **SA** still adopted a *syn* conformation after photoirradiation due to the steric bulk around the 8-thio group. On the other hand, **SH** can interact with adenine using an [A, D] H-bonding pattern on the Hoogsteen face (Fig. S5†).

Conclusions

In conclusion, we have developed 8-thiopurine nucleobase analogues bearing a photolabile NV group on the sulfur atom. The H-bonding patterns of the Hoogsteen face in SA^{NV} and SH^{NV} could be changed by photoirradiation. T_m analysis indicated that light-induced changes in the H-bonding pattern profoundly influence the base recognition ability of the nucleobase in duplex DNA. In particular, base recognition by SH^{NV} is efficiently shifted from guanine to adenine upon photoirradiation. We believe that these unique light-responsive nucleobase analogues could be powerful tools for the spatio-temporal control of DNA assembly.

Experimental

General

Reagents and solvents were purchased from commercial suppliers and were used without purification unless otherwise specified. All experiments involving air- and/or moisture-sensitive compounds were carried out under an N_2 atmosphere. All reactions were monitored with analytical TLC (Merck Kieselgel 60 F254). Column chromatography was carried out using Fuji Silysia FL-100D. Physical data were measured as follows: NMR spectra were recorded on a JEOL JNM-ECS-400 spectrometer using $CDCl_3$ or DMSO-d_6 as the solvent with tetramethylsilane as an internal standard. IR spectra were recorded on a JASCO FT/IR-4200 spectrometer. Optical rotations were recorded on a JASCO P-2200 instrument. FAB mass spectra were measured on a JEOL JMS-700 mass spectrometer. MALDI-TOF mass spectra were recorded on a Bruker Daltonics Autoflex II TOF/TOF mass spectrometer.

Synthesis of the phosphoramidite-bearing SA^{NV} and SH^{NV} nucleobase analogues

6-Nitroveratrylthiol (2). To a solution of 6-nitroveratryl bromide (1.47 g, 5.36 mmol) in dry THF (54.0 mL) was added potassium thioacetate (734 mg, 6.43 mmol) and the reaction mixture was stirred for 5 h at room temperature. The solvent was removed *in vacuo* and the residue was partitioned between AcOEt and H_2O. The separated organic layer was washed with brine and then dried (Na_2SO_4) and concentrated *in vacuo*. The resulting residue (1.52 g) was dissolved in MeOH (51.0 mL), and 35% aqueous HCl (3.20 mL) was added. After being stirred for 12 h at 60 °C, the solvent was removed *in vacuo*. The residue was purified on a silica gel column eluted with hexane–AcOEt (4 : 1 to 1 : 1) to give **2** (1.15 g, 94%) as a yellow

solid; mp 86–87 °C; ^{1}H NMR (400 MHz, $CDCl_3$) δ 7.66 (1H, s), 6.86 (1H, s, H-2 or H-5), 4.03 (2H, d, J = 8.5 Hz, SCH_2Ar), 3.99 (3H, s, Ar-OCH_3), 3.95 (3H, s, Ar-OCH_3), 2.23 (1H, t, J = 8.5 Hz, SH); ^{13}C NMR (100 MHz, $CDCl_3$) δ 153.3, 147.8, 139.6, 132.0, 112.5, 108.2, 56.3, 56.2, 27.0; IR (KBr) 2577, 1520, 1273 cm^{-1}; FAB-LRMS m/z = 252 (MNa^+); FAB-HRMS calcd for $C_9H_{11}NNaO_4S$ 252.0306, found 252.0306.

6-*N*-Benzoyl-5′-*O*-(4,4′-dimethoxytrityl)-8-(6-nitroveratrylthio)-2′-deoxyadenosine (4). To a solution of **3**[18] (300 mg, 0.408 mmol) in dry DMF (4.10 mL) were added K_2CO_3 (169 mg, 1.22 mmol) and **2** (103 mg, 0.449 mmol) at room temperature. After being stirred for 1 h at room temperature, the resulting mixture was partitioned between Et_2O and H_2O. The separated organic layer was washed with brine, dried (Na_2SO_4) and concentrated *in vacuo*. The resulting residue was purified on a silica gel column eluted with hexane–AcOEt (2 : 3 to 1 : 2 with 0.5% Et_3N) to give **4** (187 mg, 52%) as a yellow foam; ^{1}H NMR (400 MHz, $CDCl_3$) δ 8.93 (1H, brs, NH), 8.43 (1H, s, H-2), 8.04 (2H, d, J = 7.5 Hz), 7.64–7.16 (14H, m), 6.77–6.73 (4H, m), 6.27 (1H, t, J = 7.0 Hz, H-1′), 4.99–4.85 (3H, m, H-3′ and SCH_2Ar), 4.06 (1H, dd, J = 10.0 and 6.0 Hz, H-4′), 3.88 (3H, s, Ar-OCH_3), 3.76 (3H, s, Ar-OCH_3), 3.75 (3H, s, Ar-OCH_3), 3.71 (3H, s, Ar-OCH_3), 3.40–3.34 (3H, m, H-2′a and H-5′), 2.38 (1H, brs, OH), 2.33–2.26 (1H, m, H-2′b); ^{13}C NMR (100 MHz, $CDCl_3$) δ 164.7, 158.4, 158.4, 154.1, 153.2, 150.7, 148.4, 146.5, 144.7, 140.8, 135.9, 135.8, 133.8, 132.8, 130.0, 130.0, 128.9, 128.1, 128.0, 127.9, 127.8, 126.8, 123.7, 114.1, 113.0, 113.0, 108.0, 86.3, 85.7, 84.3, 72.8, 63.6, 56.4, 56.3, 55.2, 37.1, 33.6; IR (KBr) 1721 (C=O), 1521 (NO_2 as), 1274 (NO_2 sy) cm^{-1}; $[\alpha]_D^{22}$–64.8 (c 1.00, $CHCl_3$); FAB-LRMS m/z = 885 (MH^+); FAB-HRMS calcd for $C_{47}H_{45}N_6O_{10}S$ 885.2918, found 885.2928.

6-*N*-Benzoyl-5′-*O*-(4,4′-dimethoxytrityl)-3′-*O*-(*N*,*N*-diisopropyl-β-cyanoethylphosphoramidyl)-8-(6-nitroveratrylthio)-2′-deoxyadenosine (5). To a suspension of **4** (150 mg, 0.17 mmol) in dry MeCN (1.7 mL) were added *N*,*N*-diisopropylethylamine (0.089 mL, 0.51 mmol) and 2-cyanoethyl-*N*,*N*′-diisopropylchlorophosphoramidite (0.057 mL, 0.26 mmol) at room temperature. After being stirred for 30 min, the resulting mixture was partitioned between AcOEt and H_2O. The separated organic layer was washed with saturated aqueous $NaHCO_3$, followed by brine, then dried (Na_2SO_4) and concentrated *in vacuo*. The residue was purified on a silica gel column eluted with hexane–AcOEt (3 : 2 with 0.5% Et_3N) to give **5** (142 mg, 77%) as a yellow foam; ^{31}P NMR δ 141.4, 141.1; FAB-LRMS m/z = 1085 (MH^+); FAB-HRMS calcd for $C_{56}H_{62}N_8O_{11}PS$ 1085.3996, found 1085.4053.

8-(6-Nitroveratrylthio)-2′-deoxyinosine (7). To a solution of **6**[19] (1.65 g, 5.00 mmol) in dry DMF (50.0 mL) were added K_2CO_3 (829 mg, 6.00 mmol) and **2** (1.37 g, 6.00 mmol) at room temperature. After being stirred for 24 h at room temperature, the solvent was removed *in vacuo*. The residue was purified on a silica gel column eluted with AcOEt to AcOEt–MeOH (10 : 1) to give **7** (596 mg, 25%) as a yellow powder; ^{1}H NMR (400 MHz, DMSO-d_6) δ 12.5 (1H, brs, NH), 8.02 (1H, s), 7.68 (1H, s), 7.47 (1H, s), 6.14 (1H, t, J = 6.5 Hz, H-1′), 5.33 (1H, brs, OH), 4.91 (1H, brs, OH), 4.79 and 4.75 (each 1H, each d, J = 13.5 Hz, SCH_2Ar), 4.37 (1H, brs, H-3′), 3.86 (3H, s, Ar-OCH_3), 3.85 (3H, s, Ar-OCH_3), 3.81–3.77 (1H, m, H-4′), 3.60–3.57 (1H, m, H-5′a), 3.46–3.44 (1H, m, H-5′b), 2.98–2.91 (1H, m, H-2′a), 2.12–2.06 (1H, m, H-2′b); ^{13}C NMR (100 MHz, DMSO-d_6) δ 155.6, 152.6, 149.5, 147.9, 146.5, 145.2, 139.7, 127.4, 124.7, 115.3, 108.3, 88.0, 84.3, 70.9, 61.9, 56.1, 56.1, 37.2, 34.1; IR (KBr) 3366, 1686, 1523, 1275 cm^{-1}; FAB-LRMS m/z = 480 (MH^+); FAB-HRMS calcd for $C_{19}H_{22}N_5O_8S$ 480.1189, found 480.1207.

5′-*O*-(4,4′-Dimethoxytrityl)-8-(6-nitroveratrylthio)-2′-deoxyinosine (8). To a solution of **7** (560 mg, 1.17 mmol) in dry pyridine (12.0 mL) was added 4,4′-dimethoxytrityl chloride (474 mg, 1.40 mmol) at room temperature. After being stirred for 5 h at room temperature, the reaction was quenched by addition of MeOH. The resulting mixture was partitioned between AcOEt and H_2O. The separated organic layer was washed with saturated aqueous $NaHCO_3$, followed by brine, and then dried (Na_2SO_4) and concentrated *in vacuo*. The residue was purified on a silica gel column eluted with $CHCl_3$–MeOH (50 : 1 with 0.5% Et_3N) to give **8** (770 mg, 85%) as a yellow foam; ^{1}H NMR (400 MHz, $CDCl_3$) δ 7.70 (1H, s), 7.67 (1H, s), 7.53 (1H, s), 7.39 (1H, d, J = 7.5 Hz), 7.29–7.18 (1H, m), 6.78 (4H, dd, J = 8.5 and 3.0 Hz), 6.20 (1H, t, J = 6.5 Hz, H-1′), 4.95 and 4.91 (each 1H, each d, J = 13.5 Hz, SCH_2Ar), 4.76–4.74 (1H, m, H-3′), 4.02–3.99 (1H, m, H-4′), 3.97 (3H, s, Ar-OCH_3), 3.92 (3H, s, Ar-OCH_3), 3.77 (6H, s, 2 × Ar-OCH_3), 3.45–3.42 (1H, m, H-5′a), 3.35–3.31 (1H, m, H-5′b), 3.18–3.11 (1H, m, H-2′a), 2.30–2.23 (1H, m, H-2′b); ^{13}C NMR (100 MHz, $CDCl_3$) δ 158.4, 158.0, 153.1, 150.6, 150.0, 148.3, 144.6, 142.7, 139.9, 135.9, 130.0, 130.0, 128.2, 128.1, 127.7, 126.8, 124.9, 115.0, 113.0, 108.2, 86.3, 85.5, 84.2, 72.7, 63.8, 56.6, 56.3, 55.2, 37.5, 34.1; IR (KBr) 3007, 1678, 1519, 1276 cm^{-1}; FAB-LRMS m/z = 782 (MH^+); FAB-HRMS calcd for $C_{40}H_{40}N_5O_{10}S$ 782.2496, found 782.2531.

5′-*O*-(4,4′-Dimethoxytrityl)-3′-*O*-(*N*,*N*-diisopropyl-β-cyanoethylphosphoramidyl)-8-(6-nitroveratrylthio)-2′-deoxyinosine (9). To a solution of **8** (690 mg, 0.88 mmol) in dry MeCN (8.8 mL) was added *N*,*N*-diisopropylethylamine (0.46 mL, 2.7 mmol) and 2-cyanoethyl-*N*,*N*′-diisopropylchlorophosphoramidite (0.29 mL, 1.3 mmol) at room temperature. After being stirred for 30 min at room temperature, the resulting mixture was partitioned between AcOEt and H_2O. The separated organic layer was washed with saturated aqueous $NaHCO_3$, followed by brine, then dried (Na_2SO_4) and concentrated *in vacuo*. The residue was purified on a silica gel column eluted with hexane–AcOEt (1 : 4 with 0.5% Et_3N) to AcOEt : MeOH (10 : 1 with 0.5% Et_3N) to give **9** (600 mg, 74%) as a yellow foam; ^{31}P NMR δ 148.6, 148.4; FAB-LRMS m/z = 982 (MH^+); FAB-HRMS calcd for $C_{49}H_{57}N_7O_{11}PS$ 982.3574, found 982.3625.

Oligonucleotide synthesis

Solid-phase oligonucleotide synthesis was performed on an nS-8 Oligonucleotides Synthesizer (GeneDesign, Inc.) using commercially available reagents and phosphoramidites. The modified phosphoramidite was incorporated into the oligonucleotide with a coupling efficiency comparable to that

This journal is © The Royal Society of Chemistry 2014

of commercially available phosphoramidites without any modifications to the coupling conditions. Oligonucleotides were synthesized (with trityl-off) on a 500 Å CPG solid support column (0.2 μmol scale) using 5-(bis-3,5-trifluoromethylphenyl)-1*H*-tetrazole (0.25 M in MeCN) as the activator. Cleavage from the solid support and deprotection were accomplished with concentrated ammonium hydroxide solution at 55 °C for 12 h. The crude oligonucleotides were purified on a Nap 10 column (GE Healthcare) followed by RP-HPLC on a XBridge™ OST C18 column, 2.5 μm, 10 × 50 mm (Waters) using MeCN in 0.1 M triethylammonium acetate buffer (pH 7.0). The purified oligonucleotides were quantified by UV absorbance at 260 nm and confirmed by MALDI-TOF mass spectrometry.

UV melting experiments

Melting temperatures (T_m) of the oligonucleotides were determined by measuring the change in absorbance at 260 nm as a function of temperature using a SHIMADZU UV-Vis spectrophotometer UV-1650PC equipped with a TMSPC-8 T_m analysis accessory. The samples were denatured at 100 °C and annealed slowly to room temperature. The absorbance was recorded in the forward and reverse directions between 5 and 90 °C at a rate of 0.5 °C min^{-1}. T_m values of duplexes after photoirradiation were measured using samples irradiated (365 nm) at 37 °C.

Photoirradiation reaction

Photoirradiation of oligonucleotides was performed in sodium phosphate buffer (pH 7.2) at 37 °C for 5 minutes using an OMRON UV-LED lamp ZUV-C30H as the light source (365 nm) and a ZUV-L10H as the lens unit (760 mW cm^{-2}). Analyses of the photoproducts were carried out without further purification.

Acknowledgements

This work was supported by the Japan Society for the Promotion of Science (JSPS), the Ministry of Education, Culture, Sports, Science and Technology (MEXT), and the Advanced Research for Medical Products Mining Programme of the National Institute of Biomedical Innovation (NIBIO), Japan.

Notes and references

1 D. D. Young, H. Lusic, M. O. Lively, J. A. Yoder and A. Deiters, *ChemBioChem*, 2008, **9**, 2937.
2 D. D. Young, M. O. Lively and A. Deiters, *J. Am. Chem. Soc.*, 2010, **132**, 6183.
3 V. Mikat and A. Heckel, *RNA*, 2007, **13**, 2341.
4 J. M. Govan, D. D. Young, H. Lusic, Q. Liu, M. O. Lively and A. Deiters, *Nucleic Acids Res.*, 2013, **41**, 10518.
5 A. Heckel and G. Mayer, *J. Am. Chem. Soc.*, 2005, **127**, 822.
6 C. Höbartner and S. K. Silverman, *Angew. Chem., Int. Ed.*, 2005, **44**, 7305.
7 A. Nierth, M. Singer and A. Jäschke, *Chem. Commun.*, 2010, **46**, 7975.
8 H. Lusic, D. D. Young, M. O. Lively and A. Deiters, *Org. Lett.*, 2007, **9**, 1903.
9 H. Lusic, M. O. Lively and A. Deiters, *Mol. BioSyst.*, 2008, **4**, 508.
10 K. B. Joshi, A. Vlachos, V. Mikat, T. Deller and A. Heckel, *Chem. Commun.*, 2012, **48**, 2746.
11 T. L. Schmidt, M. B. Koeppel, J. Thevarpadam, D. P. N. Goncalves and A. Heckel, *Small*, 2011, **7**, 2163.
12 A. Prokup, J. Hemphill and A. Deiters, *J. Am. Chem. Soc.*, 2012, **134**, 3810.
13 J. Hemphill and A. Deiters, *J. Am. Chem. Soc.*, 2013, **135**, 10512.
14 K. Morihiro, T. Kodama, R. Waki and S. Obika, *Chem. Sci.*, 2014, **5**, 744.
15 A. Patchornik, B. Amit and R. B. Woodward, *J. Am. Chem. Soc.*, 1970, **92**, 6333.
16 M. L. Hamm, R. Cholera, C. L. Hoey and T. J. Gill, *Org. Lett.*, 2004, **6**, 3817.
17 K. Miyata, R. Tamamushi, H. Tsunoda, A. Ohkubo, K. Seio and M. Sekine, *Org. Lett.*, 2009, **11**, 605–608.
18 T. P. Prakash, R. K. Kumer and K. N. Ganesh, *Tetrahedron*, 1993, **49**, 4035.
19 R. E. Holmes and R. K. Robins, *J. Am. Chem. Soc.*, 1964, **86**, 1242.
20 I. V. Kutyavin, R. L. Rhinehart, E. A. Lukhtanov, V. V. Gorn, R. B. Meyer Jr. and H. B. Gamper Jr., *Biochemistry*, 1996, **35**, 11170.
21 J. Lohse, O. Dahl and P. E. Nielsen, *Proc. Natl. Acad. Sci. U. S. A.*, 1999, **96**, 11804.
22 G. Varani and W. H. McClain, *EMBO Rep.*, 2000, **1**, 18.

This journal is © The Royal Society of Chemistry 2014

ChemComm

COMMUNICATION

View Article Online
View Journal | View Issue

Guanidine bridged nucleic acid (GuNA): an effect of a cationic bridged nucleic acid on DNA binding affinity†

Cite this: *Chem. Commun.*, 2014, **50**, 575

Received 7th August 2013,
Accepted 5th November 2013

DOI: 10.1039/c3cc46017g

www.rsc.org/chemcomm

Ajaya R. Shrestha, Yutaro Kotobuki, Yoshiyuki Hari and Satoshi Obika*

A novel 2′,4′-BNA/LNA analog bridged by guanidine, termed as guanidine bridged nucleic acid (GuNA), was synthesized and incorporated into oligonucleotides. Thermal stabilities and nuclease resistance of GuNA-modified oligonucleotides were investigated and compared with those of 2′,4′-BNA/LNA and natural DNA oligonucleotides. GuNA exhibited interestingly high binding affinity towards complementary ssDNA than 2′,4′-BNA/LNA.

During the last few decades, many efforts have been directed towards the development of chemically modified oligonucleotides that could exhibit promising therapeutic potencies by selective targeting of disease related genes.[1] Many synthetic oligonucleotides have been developed by modifying a nucleobase, sugar and/or phosphate backbone.[2] As nucleic acid is a highly charged polyionic natural polymer, the electrostatic repulsion between the strands of duplexes and triplexes should have considerable effect on the hybridization properties of an oligonucleotide. Therefore, manipulation of the total charge of an oligonucleotide is one of the interesting strategies to improve the properties of a modified oligonucleotide. Many studies have been carried out to develop oligonucleotides with uncharged backbones, such as methylphosphonates,[3] peptide nucleic acids (PNA)[4] and phosphorodiamidate morpholino oligomers.[5] These oligonucleotides exhibited high binding affinities towards complementary strands maintaining sequence specificity, which may be attributed to the absence of charge that eliminates charge–charge repulsion. Another interesting approach to neutralize the inter-strand repulsion is to replace anionic phosphodiester groups by cationic linkages.[6,7] Also, studies have been conducted by introducing cationic tethers into the nucleobases[8,9] or to the 2′-position of the sugar moiety of a nucleic acid.[10,11] These modified oligonucleotides are reported to exhibit improved properties like enhanced binding affinities towards complementary strands and high nuclease resistance. Moreover, the cationic oligonucleotides are found to enhance cellular uptake.[12–14] Thus, the introduction of cationic moieties in an oligonucleotide can modulate the net charge of an antisense oligonucleotide which could exert positive effects on the properties of a modified oligonucleotide.

Our ongoing research on 2′,4′-bridged nucleic acid (2′,4′-BNA)[15] or locked nucleic acid (LNA)[16] and its analogs has revealed many interesting facts that are useful for improving the potencies of 2′,4′-BNA/LNA based oligonucleotides.[17] We are now interested in introducing a cationic moiety in the bridged structure of 2′,4′-BNA/LNA and study its effects on the properties of the modified oligonucleotides. Herein, we have synthesized and studied the properties of a new analog of 2′,4′-BNA/LNA, termed as guanidine bridged nucleic acid (GuNA) (Fig. 1). Its structure shares common structural properties with 2′,4′-BNA/LNA and 2′-amino LNA.[18] The five-membered bridged structure of GuNA is characterized by the presence of a guanidine moiety in its bridged structure. The guanidinium group is highly basic ($pK_a \sim 12.5$), and can possess cationic charge under physiological conditions and maintain its charge over wide pH ranges. Due to this interesting property, the guanidinium group has been used in previous reports such as deoxynucleic guanidine (DNG)[6] and guanidine-based peptide nucleic acid (GPNA),[19] to introduce positive charge in an oligonucleotide. Our approach of introducing a cationic charge in the bridged structure of 2′,4′-BNA/LNA is expected to enhance properties like cellular permeability of a modified oligonucleotide without compromising duplex stabilities and nuclease resistance.

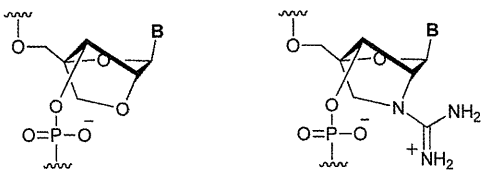

2′,4′-Bridged Nucleic Acid (2′,4′-BNA)/ Locked Nucleic Acid (LNA) | Guanidine bridged Nucleic Acid (GuNA)

Fig. 1 Structures of 2′,4′-BNA/LNA and GuNA.

Graduate School of Pharmaceutical Sciences, Osaka University, 1-6 Yamadaoka, Suita, Osaka, 565-0871, Japan. E-mail: obika@phs.osaka-u.ac.jp; Fax: +81 6 6879 8204; Tel: +81 6 6879 8200

† Electronic supplementary information (ESI) available: Experimental section and supplementary figures. See DOI: 10.1039/c3cc46017g

This journal is © The Royal Society of Chemistry 2014

The starting material for the synthesis of GuNA was 3-*O*-benzyl-4-*C*-hydroxymethyl-1,2-*O*-isopropylidene-α-D-ribofuranose **1**, a common precursor for the synthesis of 2′,4′-BNA/LNA (Scheme 1). Following a known procedure,[20,21] **2** was synthesized in nine steps from **1**. The azido group at 2′-position of **2** was reduced to an amine by sodium borohydride in the presence of nickel chloride to yield **3**. Condensation of **3** with *N*,*N*′-bis-*tert*-butoxycarbonylthiourea activated by EDCI in the presence of diisopropylethylamine yielded **4**. Desilylation of **4** by 1N TBAF in THF produced **5** in an excellent yield. The free hydroxyl moiety was triflated and the product obtained was stirred in the presence of triethylamine for 27 h to produce **6** with the desired bridged structure of the target GuNA monomer. The appearance of a singlet proton at C1′ in the ^{1}H-NMR spectrum of **6** due to the absence of coupling between hydrogens at C1′ and C2′ positions confirmed the structure of GuNA with an *N*-type sugar conformation, as observed in 2′,4′-BNA/LNA and other bridged nucleic acids.[15] Debenzylation was carried out by employing catalytic hydrogenolysis to yield the monomer **7**. For the incorporation of the GuNA monomers into oligonucleotides, the primary hydroxyl of the nucleoside **7** was protected by the 4,4′-dimethoxytrityl group to give the trityl derivative **8**. The secondary hydroxyl was then phosphitylated by 2-cyanoethyl *N*,*N*,*N*′,*N*′-tetraisopropylphosphorodiamidite to yield the GuNA-thymidine phosphoramidite **9**. The phosphoramidite was incorporated into oligonucleotides by an automated DNA synthesizer following the standard phosphoramidite protocol, except for a prolonged coupling time of 20 min. The *N*-BOC protecting groups of the synthesized GuNA-modified oligonucleotides were deprotected by 75% trifluoroacetic acid (TFA).[22] The properties of the synthesized oligonucleotides were studied and compared with those of the natural DNA and the 2′,4′-BNA/LNA-modified counterparts. To study the thermal stabilities of the GuNA-modified oligonucleotides, a set of T10-mer oligonucleotides modified with GuNA at various positions (**ON-2**–**ON-6**) were synthesized and their melting temperatures (T_m) were studied. It was found that GuNA-modified oligonucleotides possess excellent binding affinities towards complementary DNA and RNA (Table 1 and Table SI-2, ESI†). The T_m values of GuNA-modified oligonucleotides (**ON-2**–**ON-5**) with complementary RNA were comparable to those of 2′,4′-BNA/LNA-modified oligonucleotides (**ON-7**–**ON-10**). Interestingly, the T_m value dramatically increased when an oligonucleotide was modified alternatively with five GuNA monomers (**ON-6**). More interestingly, the T_m values of all of the GuNA-modified oligonucleotides with complementary DNA (ΔT_m/mod$_{(DNA-GuNA)}$ = +5 to +10.7 °C) were considerably higher than those of 2′,4′-BNA/LNA-modified oligonucleotides (ΔT_m/mod$_{(DNA-2',4'-BNA/LNA)}$ = +3 to +5 °C). In general, the modified oligonucleotide with five GuNA monomers (**ON-6**) was found to exhibit notably higher binding affinities towards complementary RNA and DNA than its 2′,4′-BNA/LNA modified counterpart. This showed that GuNA possesses an unprecedented high DNA affinity among bridged nucleic acids.[23] The result could be attributed to the presence of a cationic moiety in the bridged structure of GuNA which would create an interstrand ionic interaction in the minor groove of the DNA–GuNA double helix. This property of GuNA may have valuable applications in nucleic acid based therapeutics and technologies.

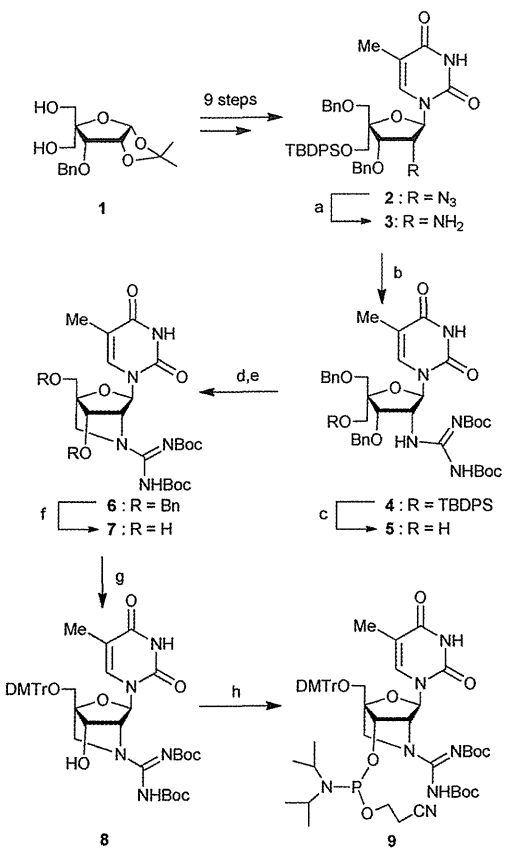

Scheme 1 Synthesis of GuNA monomer **7** and its phosphoramidite **9**. Reagents and conditions: (a) $NaBH_4$, $NiCl_2$, MeOH, rt, 76%; (b) *N*,*N*′-bis-*tert*-butoxycarbonylthiourea, EDCI, DIPEA, CH_2Cl_2, rt, 86%; (c) 1N TBAF/THF, THF, rt, quant; (d) Tf_2O, pyridine, CH_2Cl_2, 0 °C; (e) Et_3N, CH_2Cl_2, rt, 77% (2 steps); (f) H_2, $Pd(OH)_2$/C, MeOH, rt; (g) DMTrCl, pyridine, rt, 54% (2 steps); (h) $(iPr_2N)_2$-$POCH_2CH_2CN$, *N*,*N*-diisopropylammonium tetrazolide, MeCN, rt, 86%.

Table 1 T_m (°C) values of duplex formed by GuNA and 2′,4′-BNA/LNA-modified oligonucleotides with complementary ssRNA and ssDNA

	T_m (ΔT_m/mod.) (°C)	
Oligonucleotides	RNA complement	DNA complement
5′-TTTTTTTTTT-3′ (**ON-1**)	22	25
5′-TTTTXTTTTT-3′ (**ON-2**)	27 (+5.0)	30 (+5.0)
5′-TTTTXTXTTT-3′ (**ON-3**)	33 (+5.5)	42 (+8.5)
5′-TTXTXTXTTT-3′ (**ON-4**)	44 (+7.3)	57 (+10.7)
5′-TTTXXXTTTT-3′ (**ON-5**)	44 (+7.3)	55 (+10.0)
5′-XTXTXTXTXT-3′ (**ON-6**)	66 (+8.8)	77 (+10.4)
5′-TTTTYTTTTT-3′ (**ON-7**)	28 (+6.0)	25 (+0.0)
5′-TTTTYTYTTT-3′ (**ON-8**)	34 (+6.0)	31 (+3.0)
5′-TTYTYTYTTT-3′ (**ON-9**)	43 (+7.0)	40 (+5.0)
5′-TTTYYYTTTT-3′ (**ON-10**)	42 (+6.7)	35 (+3.3)
5′-YTYTYTYTYT-3′ (**ON-11**)	50 (+5.6)	48 (+4.6)

Conditions: 20 mM cacodylate buffer (pH 6.8), 200 mM KCl, 4 μM each oligonucleotide, 0.5 °C min^{-1}, 260 nm. Target strand: 3′-r(AAAAAAAAAA)-5′ (**ON-12**), 3′-d(AAAAAAAAAA)-5′ (**ON-13**), **X** = GuNA-T, **Y** = 2′,4′-BNA/ LNA-T.

This journal is © The Royal Society of Chemistry 2014